RSC Advances

PAPER

View Article Online
View Journal | View Issue

Cite this: *RSC Adv.*, 2021, **11**, 11244

Incorporation of Keggin-based $H_3PW_7Mo_5O_{40}$ into bentonite: synthesis, characterization and catalytic applications†

Dipak S. Aher, Kiran R. Khillare and Sunil G. Shankarwar *

The Keggin-based molybdo-substituted tungstophosphoric acid, $H_3[PW_7Mo_5O_{40}]\cdot 12H_2O$, were synthesized and incorporated with a bentonite clay by using a wetness impregnation method. The catalysts were characterized using several methods, such as inductively coupled plasma-atomic emission spectroscopy (ICP-AES), Fourier transform infrared spectroscopy (FT-IR), X-ray diffractometry (XRD), scanning electron microscopy energy-dispersive X-ray spectroscopy (SEM-EDS), transmission electron microscopy (TEM), and thermogravimetric and differential thermal analysis (TG-DTA). This extremely active catalytic system provides a green strategy for the synthesis of 1,8-dioxo-octahydroxanthene and 1,8-dioxo-decahydroacridine derivatives under solvent free conditions at 80 °C with a good reaction mass efficiency, effective mass yield, and excellent atom economy. Both the surface acidity and catalytic activity sharply increased after $H_3[PW_7Mo_5O_{40}]\cdot 12H_2O$ was impregnated with bentonite clay. In addition, the PW_7Mo_5/bentonite catalyst can be conveniently recovered and reused numerous times without demonstrating a significant loss in activity.

Received 12th February 2021
Accepted 26th February 2021

DOI: 10.1039/d1ra01179k

rsc.li/rsc-advances

1. Introduction

Polyoxometallates (POMs) or heteropoly acid (HPAs) are a large family of distinct d-block transitional metal-oxide, anionic cluster structures of metals, they have inspired several recent research activities in comprehensive fields of science.[1–6] POMs can, in some instances, be assembled with precise control regarding the placement of different heteroatoms such as W, Mo, or V within their molecular frameworks.[7–9] Predominantly, the Keggin-type POMs are also characteristically templated by a central tetrahedral template $\{XO_4\}$ (X = P, Si, Nb, B, Ge, *etc.*) that can have a prominent impact on the properties of the anion, these are mostly associated with a change in the charge and polarization of the metal-oxo shell.[10–15] Furthermore, one or more of the W atoms can be substituted by different heteroatoms that comprise inner transition metals, such as Co, Ni, Mo, V and so on to yield transition-metal substituted POMs.[8,15–17] This compositional modification tunes the reactivity and effects processes such as the acidity and stability of the POMs.[18,19] However, the major problems with POMs are their low thermal stability, low surface area, high solubility in polar solvents, and their recovery and reusability.[20] For the effective access the catalyst needs to be supported on a suitable support material.[21–23]

Bentonite, a clay mineral which is abundant on earth, consists of layers of two tetrahedral silica sheets sandwiching one octahedral alumina sheet.[24,25] It is well-documented that bentonite clays can be used as an efficient support owing to their common fascinating features, such as their higher surface acidity, excellent thermal stability, and effortlessly controlled structure and morphology.[26]

Multicomponent reactions (MCRs) provide a convenient approach for the rapid synthesis of complex molecules from simple starting materials, without the isolation of intermediates.[27] The MCRs have achieved significant importance in medicinal and organic chemistry,[28] because these reactions minimize the consumption of catalysts and solvents, thus permitting the minimization of waste, time, effort and cost as compared to multistep synthesis.[29,30] Xanthene derivatives have been classified as oxygen-containing molecular families, possessing a highly reactive inbuilt pyran ring.[31] In addition, they have been used as synthetic precursors for several organic compounds and dyes,[32–34] such as fluorescents and chiroptical molecular switches (examples include, rosamine, fluorone, fluorescein, rhodamine *etc.*).[33,35] The core structure of the xanthene derivatives shows a multitude of physicochemical and pharmacological properties, such as anti-inflammatory,[36] antimalarial,[37] analgesic,[38] anticancer,[20] antiviral,[39] antibacterial properties, and so on.[38] Additionally, acridine derivatives, constituting a 1,4-dihydropyridine (DHP) ring skeleton, are very important compounds owing to their pharmacological properties.[40] Various members of this family are currently used for cytostatic and antitumor activities (for example, nitracrine

Department of Chemistry, Dr Babasaheb Ambedkar Marathwada University, Aurangabad 431004, MS, India. E-mail: shankarwar_chem@yahoo.com

† Electronic supplementary information (ESI) available. See DOI: 10.1039/d1ra01179k

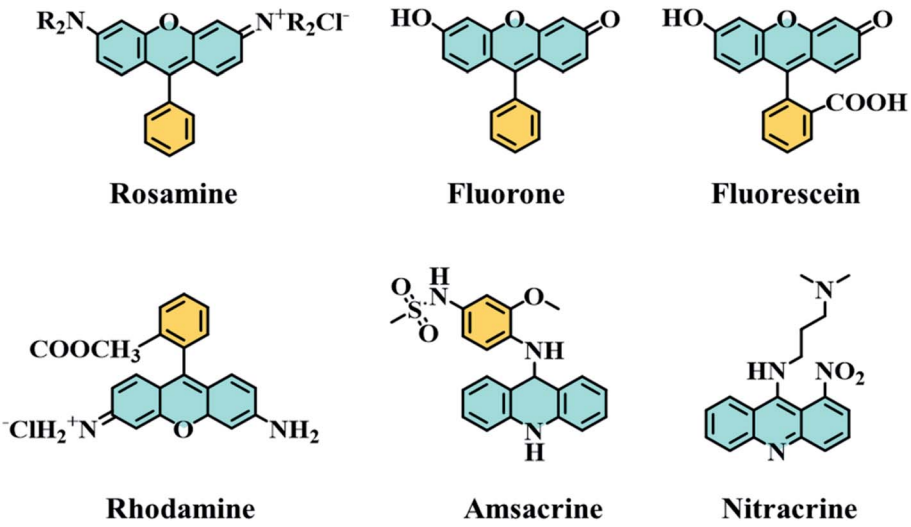

Fig. 1 Structures of some known xanthenes and acridines.

derivatives),[41] platelet antiaggregatory activities, the treatment of Alzheimer's disease, strong anti-cancer treatments (for example, amsacrine derivatives), cardiovascular diseases including hypertension and diabetes, and so on.[41,42] The structures of some xanthene and acridine derivatives are shown in Fig. 1.

As yet, several procedures have been employed for synthesizing many of these organic derivatives using various catalysts, such as Fe^{3+} montmorillonite,[43] NiFeTi CLDH6,[42] $SmCl_3$,[44] $HClO_4$–SiO_2,[45] $InCl_3$/ionic liquid,[46,47] FSG-Hf$(NPf_2)_4$,[48] *p*-dodecylbenzenesulfonic acid, Amberlyst-15,[49] $[MIMPS]_3PW_{12}O_{40}$ and $[TEAPS]_3PW_{12}O_{40}$,[47] SO_4^{2-}/ZrO_2,[50] $[Hbim]BF_4$,[51] $[Cmmim][BF_4]$,[52] SBSSA,[53] [Hmim]TFA,[54] $CaCl_2$,[55] SBNPSA,[56] thiourea dioxide,[57] $SbCl_3/SiO_2$,[58] and 2,4,6-trichloro-1,3,5-triazine (TCT).[59] However, these types of catalyst possesses some disadvantages, such as an inability to recycle the catalyst, the use of expensive reagents, use of reflux conditions, prolonged work up, hazardous organic solvents and low reaction yields. Therefore, it has become important to find an alternative route for the synthesis of xanthene and acridine derivatives. Hence, the development of a novel, contemporary reaction that is easy to perform, cost effective, and offers the reusability of the catalyst, and perhaps offers a greener method, is highly attractive.

In this regard, and in a continuation of our interest in the development of modified novel Keggin-type POMs for different acid catalysed organic transformations,[60,61] herein, we report a series of molybdo-substituted tungstophosphoric acid $H_3[PW_7Mo_5O_{40}]\cdot 12H_2O$ catalysts that were prepared and impregnated with bentonite clay (Scheme 1). Their effectiveness was explored for the preparation of 1,8-dioxo-octahydroxanthene and 1,8-dioxo-decahydroacridine derivatives in excellent yields and with a short reaction time.

2. Results and discussion

2.1 Catalytic characterization

2.1.1 FT-IR analysis. The Fourier transform infrared spectroscopy (FT-IR) spectra of the bulk PW_7Mo_5, bentonite clay and PW_7Mo_5/bentonite composites with PW_7Mo_5 loading from 10–25% are depicted in Fig. 2. For the bulk PW_7Mo_5, the characteristic bands exhibited at 1070 ($P–O_a$ in central tetrahedral),

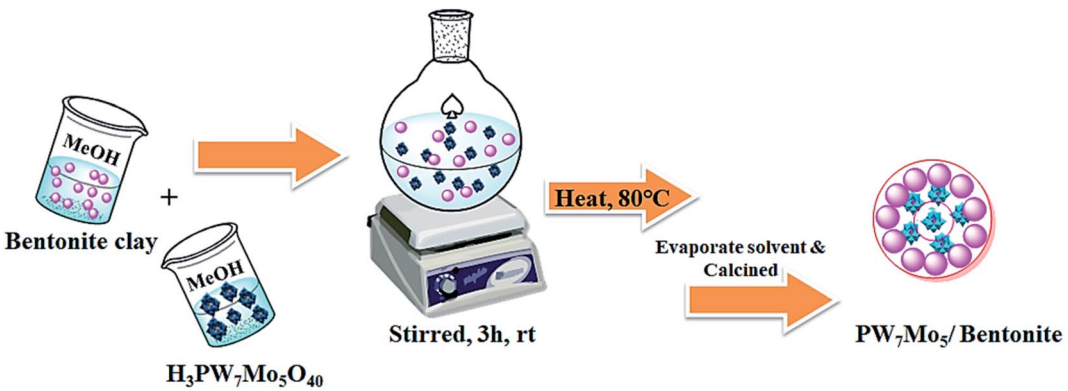

Scheme 1 Schematic illustration showing the synthetic procedure for the fabrication of the PW_7Mo_5/bentonite catalyst.

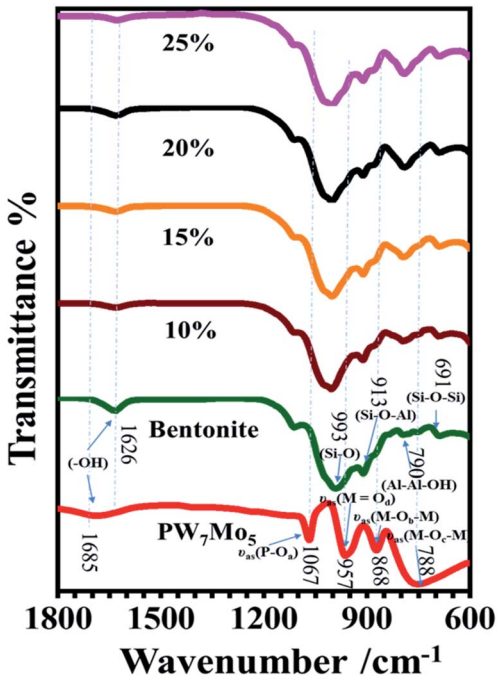

Fig. 2 FT-IR analysis of bulk PW_7Mo_5, bentonite and the PW_7Mo_5/bentonite catalyst.

958 (terminal M=O_d), 873 (M–O_b–M), and 762 cm^{-1} (M–O_c–M) coincide with the asymmetric vibrations in the Keggin unit.[17] The strong characteristic bands of the Si–O stretching vibrations were detected at 993 cm^{-1} and the bending vibration of Al–Al–OH was determined at 913 cm^{-1} for the parent bentonite. Additionally, the other two bands at 790 and 691 cm^{-1} correspond to the Si–O–Al and Si–O–Si bending vibrations, respectively.[25] However, the characteristics peaks of the 10%, 15%, 20% and 25% PW_7Mo_5 supported bentonite clays have a similar pattern to that of the parent bentonite, as only small shifts in frequency appeared owing to the electrostatic interactions between the Keggin structure of PW_7Mo_5 and the parent bentonite.[22,62]

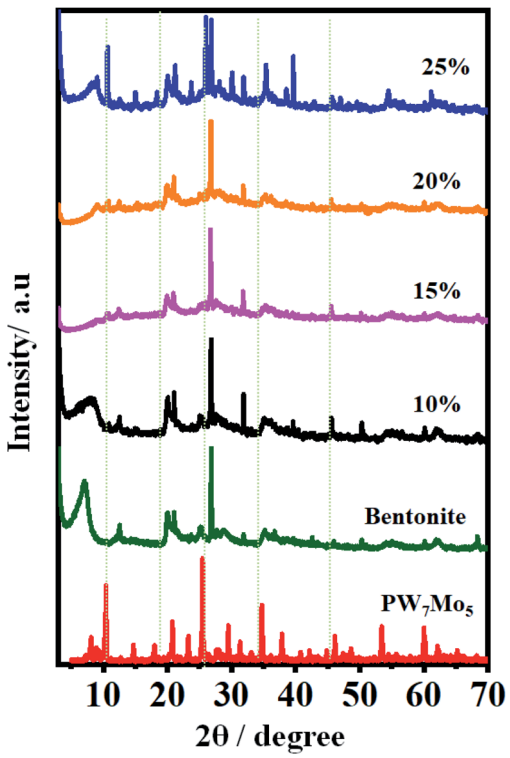

Fig. 3 XRD analysis of bulk PW_7Mo_5, bentonite and the PW_7Mo_5/bentonite catalyst.

2.1.2 XRD analysis. The X-ray diffractometry (XRD) analysis of the bulk PW_7Mo_5, plain bentonite and PW_7Mo_5/bentonite composites (with PW_7Mo_5 loading from 10, 15, 20 and 25%) in $3° < 2\theta < 80°$ are depicted in Fig. 3. The bulk PW_7Mo_5 catalyst exhibited major diffraction peaks, for example 2θ, at 7–10°, 14.5°, 20.7°, 25.44° and 34.4°, demonstrating the characteristic features of the Keggin structure and the crystalline state.[17] Sharp reflections exhibited at $2\theta = 7°$ and 20° are characteristic of the amorphous material of plain bentonite, and the one at $2\theta = 27°$ corresponds to α-quartz. For the XRD patterns of the different loading values (10, 15, 20 and 25%) of PW_7Mo_5 on bentonite, the peaks were observed to be less intense, demonstrating that during the impregnation of PW_7Mo_5 on bentonite, the clay lost some of its crystallinity compared to the parent bentonite. Most of the diffractograms of PW_7Mo_5/bentonite indicate that no separate crystal phases were detected and the 2θ value of quartz was unaffected, even after exchanging the bentonite clay with PW_7Mo_5.[26,63] This indicates that PW_7Mo_5 was well distributed over the surface of bentonite.

2.1.3 SEM and TEM analysis. The surface morphology and texture of the prepared samples were examined using scanning electron microscopy (SEM) and transmission electron microscopy (TEM) analysis (Fig. 4a–d). Fig. 4a shows the agglomerated irregular-shaped crystalline structure with smooth particles for bulk PW_7Mo_5 at 2 μm magnification. The SEM images of bentonite and 20% PW_7Mo_5/bentonite are depicted in Fig. 4b and c respectively. The result clearly reveals that the surface morphology of the 20% PW_7Mo_5/bentonite catalyst is quite dissimilar from that of the parent bentonite clay. Subsequently, it was confirmed that PMo_7W_5 are homogeneously dispersed over the surface of bentonite.

In addition, the morphology of the 20% PW_7Mo_5/bentonite samples was investigated using TEM. The smaller cloudy-like features and dark coloured spot in Fig. 4 indicate that the functional components of PW_7Mo_5 were successfully immobilized and aggregate with the bentonite clay support.

2.1.4 EDX analysis and elemental mapping images. The chemical compositions of the bulk PW_7Mo_5 and 20% PW_7Mo_5/bentonite were confirmed using energy-dispersive X-ray spectroscopy (EDS) analysis as shown in Fig. S1.† The results obtained for the fresh PW_7Mo_5 catalyst clearly show the occurrence of P, W and Mo (Fig. S1a†). Furthermore, the EDX analysis of 20% PW_7Mo_5/bentonite (Fig. S1b†) showed the presence of P, W, Mo, Na, Ca, Al and O elements, confirming the formation of 20% PW_7Mo_5/bentonite.

Additionally, the elemental mapping images (EDS) of the catalyst proved the uniform distribution of the elements such

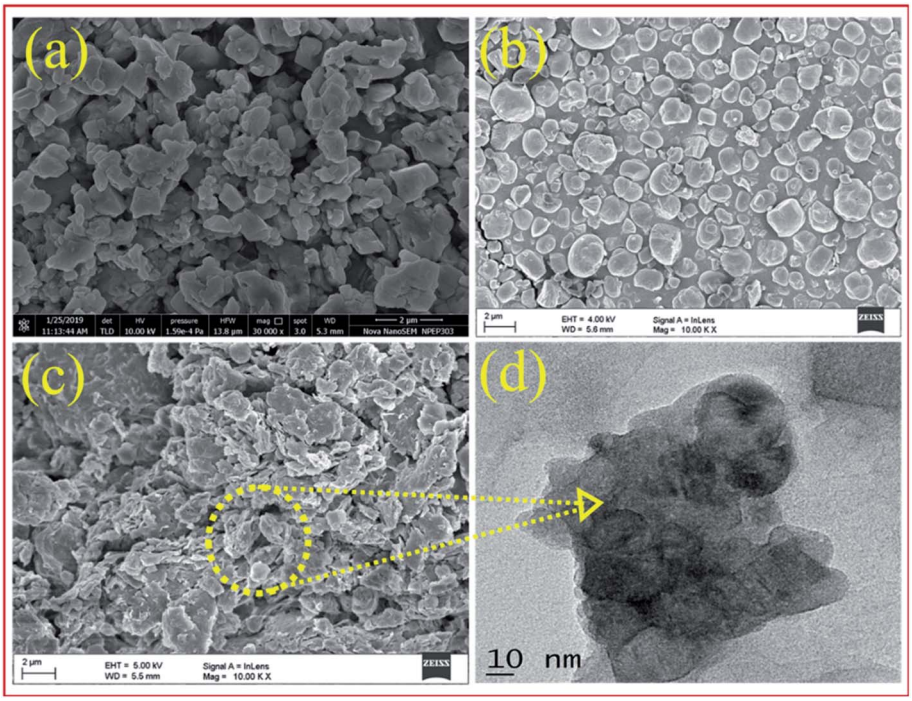

Fig. 4 FE-SEM images of bulk PW_7Mo_5 (a), bentonite clay (b), 20% PW_7Mo_5/bentonite (c) and the TEM images of 20% PW_7Mo_5/bentonite (d).

as W, Mo, P, Na, Ca, Al and O in the prepared bulk PW_7Mo_5 and the 20% PW_7Mo_5/bentonite catalyst (Fig. S2a and b†).

2.1.5 TG-DT analysis. The thermal stability of bulk PW_7Mo_5 and 20% PW_7Mo_5/bentonite were studied using thermogravimetric and differential thermal analysis (TG-DT) (Fig. 5). The three types of crystallographic water molecule obtained in the POMs are hydration water, protonized water and structural water, as depicted in Fig. 7.[17,60] The TG curve for the bulk PW_7Mo_5 shows the total weight loss of 8.78% below 520 °C, which demonstrates that 12-water molecules were lost. The first mass loss at 70 to 150 °C, was about 7.38% because of the loss of the absorbed water molecule. The second weight loss of 2.92% appeared as an endothermic peak at 350 °C for 2.18 molecules of protonized water. The third exothermic peak appeared at

Table 1 Effect of PW_7Mo_5 loading on the support bentonite for the model reaction[a]

Entry	Catalyst	Time[b] (min)	Yield[c] (%)
1	Pure bentonite	85	65
2	Bulk $H_3PW_7Mo_5O_{40}\cdot 12H_2O$	45	70
3	10% PW_7Mo_5/bentonite	35	70
4	15% PW_7Mo_5/bentonite	15	85
5	**20% PW_7Mo_5/bentonite**	**5**	**92**
6	25% PW_7Mo_5/bentonite	5	92

[a] Reaction conditions: 1 : 2 ratio of benzaldehyde, 5,5-dimethyl-1,3-cyclohexanedione and different catalysts (100 mg) at 80 °C. [b] Reaction progress monitored by TLC. [c] Isolated yields, bold values highlight the best result.

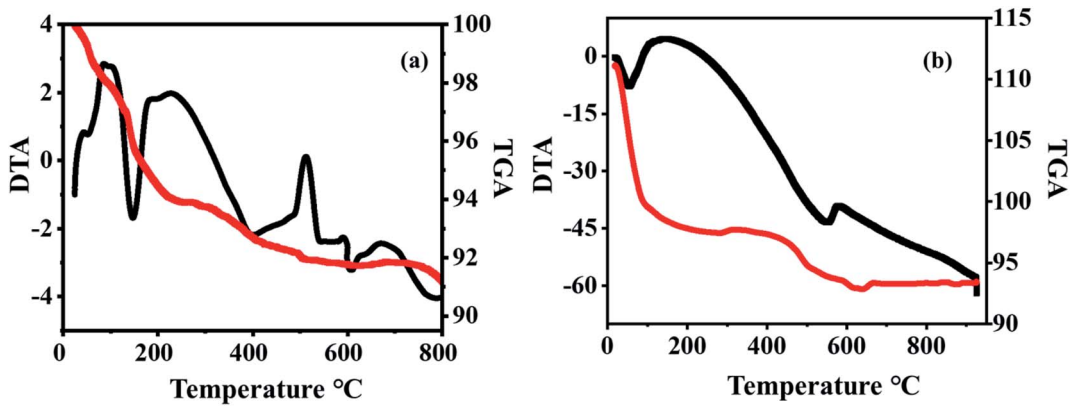

Fig. 5 TG-DT analysis of (a) PW_7Mo_5 and (b) the 20% PW_7Mo_5/bentonite catalyst.

520 °C, owing to the weight loss of 1.2% for the structural water molecule. The exothermic peak centred at 520 °C is attributed to the decay of the Keggin unit of PW_7Mo_5 to the individual oxides, suggesting that the POMs will persist up to 520 °C (Fig. 5a).

The thermogravimetric analysis (TGA) of 20% PW_7Mo_5/bentonite shows a weight loss at 80 to 175 °C, of about 9.8% owing to the weight loss of the adsorbed water molecules. A gradual mass loss of about 3% is observed up to 630 °C, which is due to the release of structural water. From this it can be seen that the thermal stability of the bulk PW_7Mo_5 materials has noticeably improved, which may be due to the strong interaction between PW_7Mo_5 and bentonite clay (Fig. 5b).[14]

2.2 Catalytic activity test

The catalytic activity of the newly prepared PW_7Mo_5/bentonite was explored for the synthesis of substituted xanthenes. Moreover, to accomplish the best reaction conditions for the xanthene synthesis, the effect of PW_7Mo_5/bentonite loading, the amount of PW_7Mo_5/bentonite, the results in various solvents, different temperatures and comparison of different catalysts were obtained. A model reaction between benzaldehyde and 5,5-dimethyl-1,3-cyclohexanedione was studied to optimize these parameters.

For a demonstration of the effect of the PW_7Mo_5 catalyst loading on bentonite for the synthesis of **3a**, different catalyst loadings were employed, such as the parent bentonite, bulk PW_7Mo_5, 10%, 15%, 20%, and 25% w/w, as shown in Table 1. The parent bentonite gave a moderate yield of the product, but it took longer for the reaction to reach completion (Table 1, entry 1). Bulk PW_7Mo_5 gave a reasonable catalytic ability in terms of the reaction time and the yield of the desired product (Table 1, entry 2). It was observed that both the yield of the product and the reaction time improved upon increasing the catalyst loading up to 20% w/w (Table 1, entries 3–5). Additionally, an increase in the amount of catalyst does not affect the reaction time and the yield of the product as a result of the leaching of the catalyst from the support (Table 1, entry 6).

Next, we performed the model reaction using various amounts of 20% PW_7Mo_5/bentonite to assess the effect of the catalyst on the synthesis of xanthene derivatives at 80 °C. It was observed that in the absence of a catalyst, product **3a** was only afforded in trace amounts (Table 2, entry 1), even after 3 h. By increasing the amount of the catalyst up to 100 mg, a notable alteration was observed in the percentage yield (Table 2, entries 2–4). There is no significant improvement in the yield observed upon increasing the amount of 20% PW_7Mo_5/bentonite catalyst up to 120 mg, because the additional catalyst does not increase the rate of the reaction (Table 2, entry 9).

Hereafter, the effects of the temperature and time were studied, which play an important role and affect the reaction kinetics to a large extent. Various temperatures (50–100 °C) were used to carry out the model reaction for different time periods (5–180 min). Hence, the best result was obtained in the presence of 100 mg of 20% PW_7Mo_5/bentonite at 80 °C (Table 2, entry 5). It was observed that no substantial change was detected after extending the reaction time and increasing the temperature.

Table 2 Optimization of the reaction conditions for the model reaction[a]

Entry	Catalyst (mg)	Temperature (°C)	Time[b] (min)	Yield[c] (%)
1	—	80	180	Trace
2	20	80	120	55
3	50	80	75	60
4	80	80	65	75
5	**100**	**80**	**5**	**92**
6	100	50	55	80
7	100	70	50	83
8	100	100	5	92
9	120	80	10	92

[a] Reaction conditions: 1 : 2 ratio of benzaldehyde, 5,5-dimethyl-1,3-cyclohexanedione and 20% PW_7Mo_5/bentonite. [b] Reaction progress monitored by TLC. [c] Isolated yields, bold values represent the best result.

Table 3 Effect of different solvents on the model reaction[a]

Entry	Solvent	Temperature (°C)	Time[b] (min)	Yield[c] (%)
1	MeOH	Reflux	25	55
2	EtOH	Reflux	20	65
3	EtOH–H_2O (1 : 1)	Reflux	10	68
4	PEG-400	110	35	75
5	CH_3CN	Reflux	5	45
6	PhMe	Reflux	25	35
7	**Solvent free**	**80**	**5**	**92**

[a] Reaction conditions: 1 : 2 ratio of benzaldehyde, 5,5-dimethyl-1,3-cyclohexanedione and 20% PW_7Mo_5/bentonite (100 mg). [b] Reaction progress was monitored by TLC. [c] Isolated yields, bold values highlight the best result.

To study the advantages of the solvent-free reaction conditions over various organic solvents, the model reaction was performed in dissimilar solvents and the results are represented in Table 3. If MeOH, EtOH, EtOH–H_2O (1 : 1), and polyethylene glycol (PEG-400) are used as the solvents, moderate yields of the products are obtained (Table 3, entries 1–4), whereas, if CH_3CN and PhMe are used, a poor yield of the product is obtained (Table 3, entries 5 and 6). However, when the reaction was carried out under thermal solvent-free conditions, a superior yield of the product was obtained within a short reaction time.

To further extend the reaction scope of the catalyst, the synthesis of 1,8-dioxo-octahydroacridines (Table 4) was carried out under the same reaction conditions as used for the synthesis of the corresponding 1,8-dioxo-octahydroxanthenes. We carried out the reaction in a 1 : 2 : 1 ratio of aldehydes, 5,5-dimethyl-1,3-cyclohexanedione and ammonium acetate (NH_4OAc) with 20% PW_7Mo_5/bentonite at 80 °C, which afforded the 1,8-dioxo-decahydroacridine derivatives (**4a–4n**) in excellent yields (92–79%) within a short period of time (Table 5). In addition, the aromatic aldehydes containing both electron withdrawing and electron donating groups afforded the

Table 4 Synthesis of 1,8-dioxo-octahydroxanthenes using the 20% PW_7Mo_5/bentonite catalyst[a,b,c]

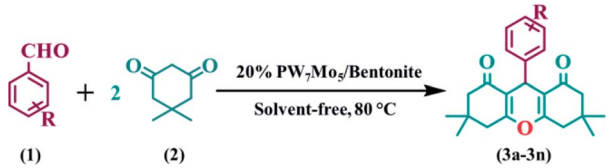

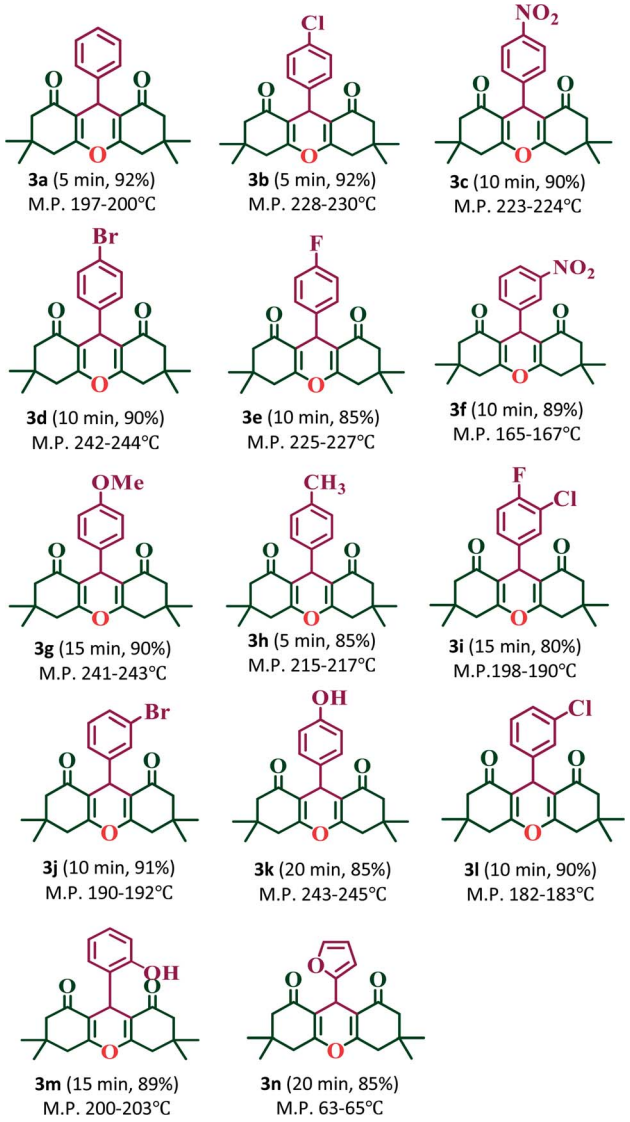

[a] Reaction conditions: 1 : 2 ratio of aldehyde, 5,5-dimethyl-1,3-cyclohexanedione and 20% PW_7Mo_5/bentonite (100 mg) stirred at 80 °C. [b] Isolated yields. [c] Melting points.[31,42,43,52]

Table 5 Synthesis of 1,8-dioxo-decahydroacridines using the 20% PW_7Mo_5/bentonite catalyst[a,b,c]

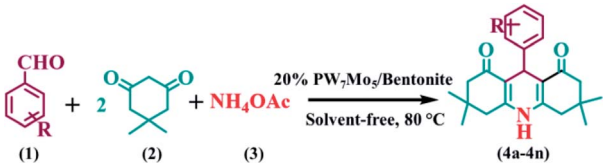

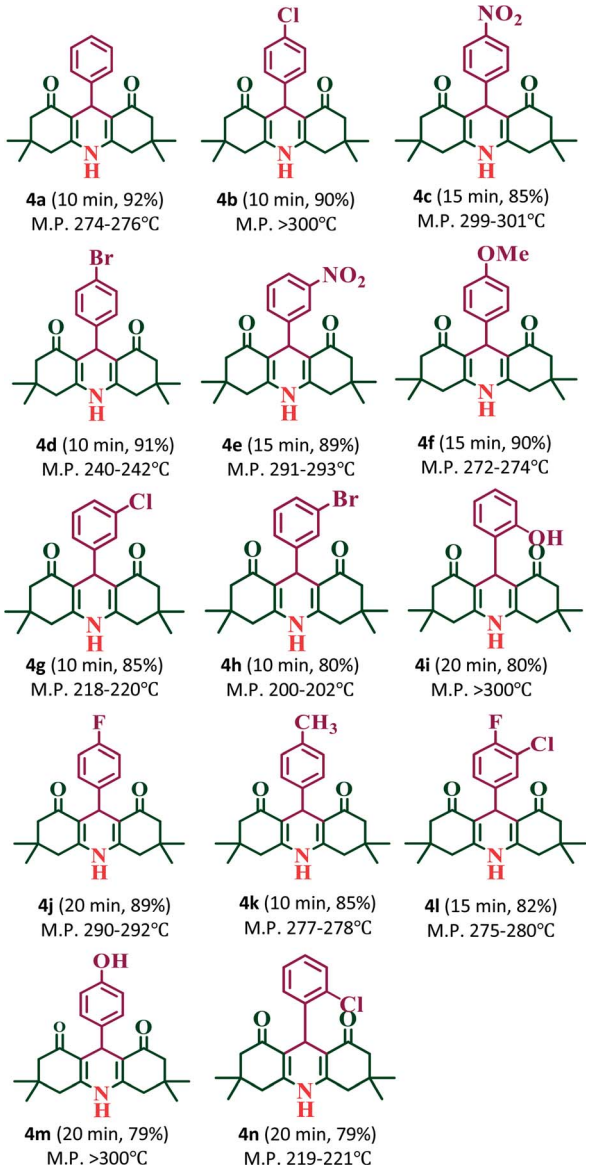

[a] Reaction conditions: 1 : 2 : 1 ratio of aldehydes, 5,5-dimethyl-1,3-cyclohexanedione, NH_4OAc and 20% PW_7Mo_5/bentonite (100 mg) stirred at 80 °C. [b] Isolated yields. [c] Melting points.[48,49,64–66]

products with high yields. The work-up procedure was very simple and included the addition of hot ethanol at the end of the reaction, filtering the reaction mixture to separate off the catalyst, and finally recrystallizing the products from ethanol.

Quantification of the effectiveness of a reaction with the aim of waste reduction continues to drive the development of novel green chemistry metrics, such as the *E*-factor, atom economy, reaction mass efficiency, optimum efficiency, and practical mass yield.[67,68] These metrics serve to quantify the efficiency or environmental performance of a chemical reaction.[69]

The *E*-factor is the mass ratio of waste to desired product and the atom efficiency.[70] The lower the value of the *E*-factor, the

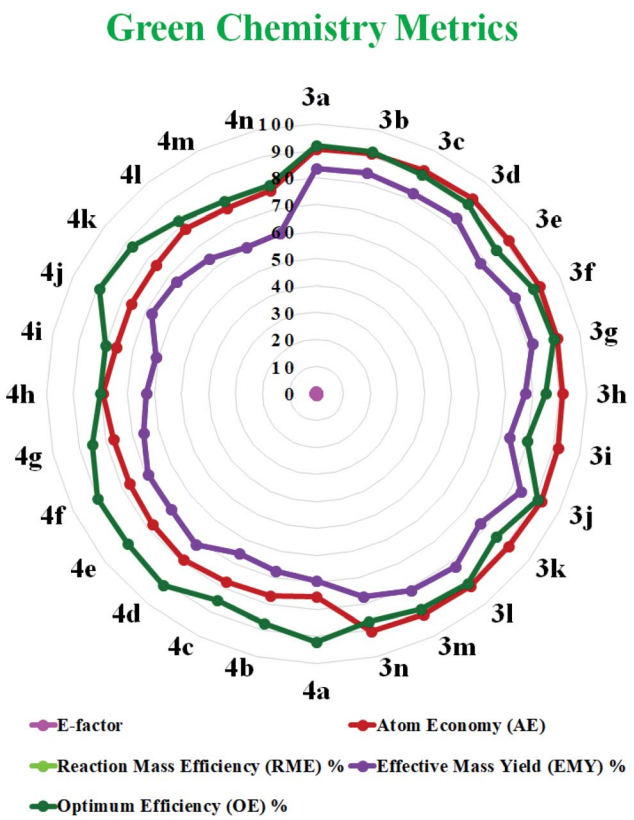

Fig. 6 Radar chart of the measured green metrics for the synthesis of 1,8-dioxo-octahydroxanthene (**3a–n**) and the 1,8-dioxo-decahydroacridine derivatives (**4a–n**).

more ecocompatible the reaction. An *E*-factor ranging from 0.1 to 0.6 highlights the greenness of the protocol, as shown in Fig. 6.

We measured the green chemistry metrics for both the 1,8-dioxo-octahydroxanthenes and 1,8-dioxo-octahydroacridines derivatives to afford **3a** and **4a** under the optimized reaction conditions and compared these with their ideal value, as demonstrated in Table 6. The result shows that the values of the green chemistry metrics such as the *E*-factor, atom economy (AE), reaction mass efficiency (RME), effective mass yield (EMY) and optimum efficiency (OE) are close to their ideal values, as demonstrated here (see the ESI† for detailed calculations).

A comparison of the catalytic efficiency of the 20% PW_7Mo_5/bentonite catalyst was performed with other reported catalysts for the synthesis of the 1,8-dioxo-octahydroxanthene

Table 6 Quantitative evaluation of green chemistry metrics for **3a** and **4a**

Entry	Green chemistry metrics	Ideal value	Product **3a**	Product **4a**
1	*E*-Factor	0	0.19	0.44
2	Atom economy (AE)	100%	90.67	75.38
3	Reaction mass efficiency (RME)	100%	83.39	69.34
4	Effective mass yield (EMY)	100%	83.39	69.34
5	Optimum efficiency (OE)	100%	91.97	91.98

Table 7 Comparative study of 20% PW_7Mo_5/bentonite with previously reported catalysts for the model reaction

Entry	Catalyst	Reaction conditions	Time	Yield (%) Ref.
1	Fe^{3+} montmorillonite	EtOH, 100 °C	6 h	94 (ref. 43)
2	SO_4^{2-}/ZrO_2	EtOH, 70 °C	8 h	95 (ref. 50)
3	$[Hbim]BF_4$	MeOH, rt	45 min	85 (ref. 51)
4	$[Cmmim][BF_4]$	Solvent free, 80 °C	150 min	87 (ref. 52)
5	SBSSA	Reflux, EtOH	10 h	98 (ref. 53)
6	[Hmim]TFA	Solvent free, 80 °C	3 h	85 (ref. 54)
7	$CaCl_2$	DMSO/85–90 °C	4 h	85 (ref. 55)
8	SBNPSA	Reflux, EtOH	2 h	93 (ref. 56)
9	Thiourea dioxide	Reflux	45 min	96 (ref. 57)
10	$SbCl_3/SiO_2$	Solvent-free, 120 °C	50 min	93 (ref. 58)
11	2,4,6-Trichloro-1,3,5-triazine (TCT)	Solvent-free, 120 °C	50 min	92 (ref. 59)
12	20% PW_7Mo_5/bentonite	Solvent free, 80 °C	5 min	92 (This work)

derivatives. The result shows that 20% PW_7Mo_5/bentonite is superior to some of the previous reported catalysts in terms of the excellent yield and short reaction time (Table 7, entry 12).

2.3 Plausible mechanism for the reaction

The 20% PW_7Mo_5/bentonite catalyses the synthesis of the 1,8-dioxo-octahydroxanthene derivatives by stimulating the carbonyl group of the aromatic aldehydes (**1**), making it more liable to nucleophilic attack by dimedone (**2**), to form intermediate (**a**), followed by Michael addition of another molecule of dimedone to form the intermediate (**b**). Intramolecular cyclization occurs after the successive removal of water, which results in the desired product (**3a–3n**) and regenerates the 20% PW_7Mo_5/bentonite catalyst in the reaction mixture (Fig. 7).

2.4 Recyclability of the 20% PW_7Mo_5/bentonite catalyst

To study the reusability of the catalyst (20% PW_7Mo_5/bentonite), recycling studies were performed using a 1 : 2 ratio of benzaldehyde, 5,5-dimethyl-1,3-cyclohexanedione and 20% PW_7Mo_5/bentonite catalyst (100 mg), which were observed to be the optimized reaction conditions for a specified time period. After the reaction reached completion (monitored by thin layer chromatography (TLC)), the reaction mixture was diluted using hot ethanol (10.0 mL) and filtered to separate the catalyst. The crude product was obtained by solvent evaporation under reduced pressure and recrystallized from ethanol. The recovered catalyst was washed with ethanol (10 mL) and dried overnight for further reuse. The results (Table 8) reveal that the catalyst stability was maintained for up to six cycles. After the sixth cycle, the recovered catalyst was characterized using FT-IR and powder XRD analysis. The characteristic peaks at 1623, 1005, 913, 787 and 687 cm^{-1} for the FT-IR spectra (Fig. S3a†)

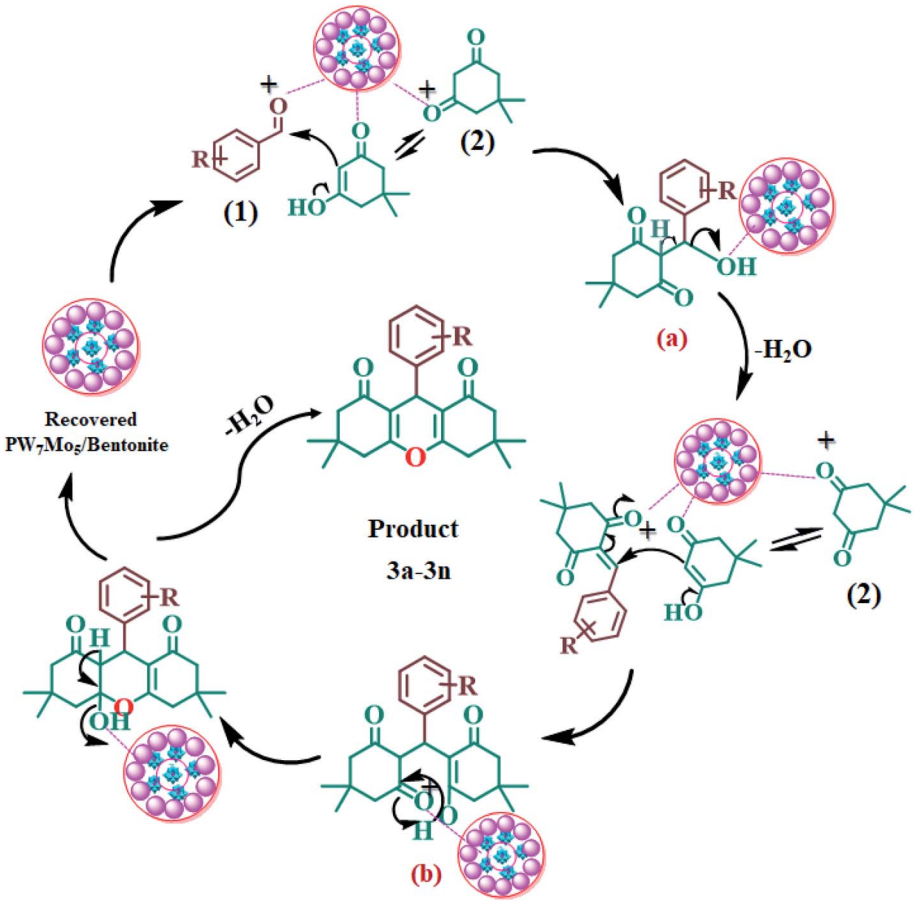

Fig. 7 Probable mechanism for the synthesis of 1,8-dioxo-octahydroxanthenes using the 20% PW_7Mo_5/bentonite catalyst.

Table 8 Recycling study of the catalyst for the model reaction[a]

No. of runs	Time[b] (min)	Yield[c] (%)
1	5	92
2	5	92
3	5	91
4	5	89
5	5	87
6	5	85

[a] Reaction conditions: 1 : 2 ratio of benzaldehyde, 5,5-dimethyl-1,3-cyclohexanedione and 20% PW_7Mo_5/bentonite (100 mg). [b] Reaction progress monitored by TLC. [c] Isolated yield.

and $2\theta = 20.70°$, 24.88°, 26.89°, and 31.63° for the XRD pattern (Fig. S3b†) remained the same.

3. Experimental

3.1 Materials and general characterization

Sodium molybdate ($Na_2MoO_4 \cdot 2H_2O$), sodium tungstate ($Na_2WO_4 \cdot 2H_2O$), disodium phosphate (Na_2HPO_4), and bentonite clay powder were purchased from Molychem in India and used without further purification. All the chemicals and solvents used in the organic synthesis were purchased from Alfa Aesar, Merck and Sigma-Aldrich.

The elemental content was measured using inductively coupled plasma-atomic emission spectroscopy (ICP-AES), ARCOS, on a simultaneous ICP Spectrometer. The FT-IR spectra were obtained using a Bruker ALPHA (Eco-ATR) spectrophotometer. The XRD pattern was obtained using a Bruker AXS Company, D8 ADVANCE diffractometer (Germany). Scanning electron microscopy (SEM) images and elemental analysis of the catalyst were employed using a FEI Nova NanoSEM 450 combined with a Bruker XFlash 6I30 instrument for energy-dispersive X-ray spectroscopy (EDX), with a scanning electron electrode at 15 kV. TEM was performed on a HR-TEM: Jeol/JEM 2100 at 200 kV voltage. TG and DTA were performed on a SHIMADZU, DTG-60H simultaneous DTA-TG apparatus. TLC was used to monitor the reaction on Merck silica plates, and the imaging was accomplished using iodine/ultraviolet light. The melting points of all the synthesized compounds were determined in open capillary tubes and are uncorrected. The ^1H NMR and ^{13}C NMR spectra were recorded on a Bruker Avance DRX-400, in pure DMSO-d_6 or $CDCl_3$ solvents using TMS as an internal reference standard.

3.2 Catalyst preparation

Synthesis of the Keggin type POMs with the general formula $H_3[PW_7Mo_5O_{40}] \cdot 12H_2O$ was performed according to a previous

report by Huixiong.[8] Briefly, disodium phosphate (0.58 g, Na_2HPO_4) and the desired amount of sodium tungstate (9.46 g, $Na_2WO_4 \cdot 2H_2O$) were dissolved in deionised water (DI). The resulting mixture was stirred for 30 min at 90 °C. Then, an aqueous solution of sodium molybdate (4.95 g, $Na_2MoO_4 \cdot 2H_2O$) was added to the above heated solution, and the pH was maintained close to 1.5–2 using sulfuric acid (H_2SO_4). The mixture was heated at 90 °C for 6 h. Finally, the cooled solution was extracted with diethyl ether. The powder $H_3[PW_7Mo_5O_{40}] \cdot 12H_2O$ was obtained after the concentrated etherate solution was dried in a vacuum. The results of the ICP-AES elemental analysis revealed that the atomic ratio of P/W/Mo is almost maintained at 1.12/7.12/5.01 which corresponds to the formula $H_3[PW_7Mo_5O_{40}] \cdot 12H_2O$ (PW_7Mo_5).

In a typical synthesis of 10% PW_7Mo_5/bentonite, 0.5 g of PW_7Mo_5 was dissolved in dry methanol solution and added dropwise into the flask containing 4.5 g of bentonite clay and stirred for 3 h at room temperature. The resulting mixture was heated to 80 °C until complete evaporation of the liquid part had occurred. The solid residue was then calcined in an oven at 200 K for 5 h. A series of PW_7Mo_5/bentonite loadings (10, 15, 20, 25 wt%) were prepared using a similar method.

3.3 General procedure for synthesis of the 1,8-dioxo-octahydroxanthene derivatives

A mixture of aromatic aldehyde (3.0 mmol), 5,5-dimethylcyclohexane-1,3-dione (6.0 mmol), and 20% PW_7Mo_5/bentonite catalyst (100 mg) was heated at 80 °C under solvent-free conditions for a suitable time, as indicated by TLC. After the reaction was complete, the reaction mixture was diluted using hot ethanol (10.0 mL) and filtered for catalyst separation. The crude product was obtained by solvent evaporation under reduced pressure and recrystallized from ethanol. The recovered catalyst was washed with ethanol (10 mL) and dried overnight for further reuse. Recrystallized xanthene derivatives were characterized using FT-IR, ^{1}H and ^{13}C NMR spectroscopy. The NMR spectral data for product **3a**, synthesized using the model reaction, are given below; the remaining spectroscopic data are provided in the ESI.†

3.3.1 3,3,6,6-Tetramethyl-9-phenyl-3,4,5,6,7,9-hexahydro-1*H*-xanthene-1,8(2*H*)-dione (3a). IR (ATR, ν cm^{-1}): 685, 835, 1035, 1242, 1364, 1581, 1664, 2958. ^{1}H NMR (400 MHz, $CDCl_3$) δ_H (ppm) = 1.09 (s, 6H, 2 × CH_3), 1.23 (s, 6H, 2 × CH_3), 2.37 (m, 8H, 4 × CH_2), 5.54 (s, 1H, CH), 7.09 (d, J = 8.2 Hz, 2H, Ar-H), 7.22 (t, 1H, Ar-H), 7.26 (t, J = 8.4 Hz, 2H, Ar-H). ^{13}C NMR (100 MHz, $CDCl_3$) δ_C (ppm) = 27.5, 29.8, 31.5, 32.8, 46.5, 47.1, 115.7, 125.9, 126.8, 128.3, 138.1, 189.6, 190.6.

3.4 General procedure for synthesis of the 1,8-dioxo-decahydroacridine derivatives

A mixture of aromatic aldehyde (3.0 mmol), 5,5-dimethylcyclohexane-1,3-dione (6.0 mmol), ammonium acetate (NH_4OAc, 3.0 mmol) and the 20% PW_7Mo_5/bentonite catalyst (100 mg) was heated at 80 °C under solvent-free conditions for a suitable time as indicated by TLC. After the reaction was complete, the reaction mixture was diluted using hot ethanol (10.0 mL) and filtered for catalyst separation. The crude product was obtained by solvent evaporation under reduced pressure and recrystallized from ethanol. The recovered catalyst was washed with ethanol (10 mL) and dried overnight for further reuse. The recrystallized xanthene derivatives were characterized using FT-IR, ^{1}H and ^{13}C NMR spectroscopy. The NMR spectral data for product **4a** are given below; the remaining spectroscopic data are provided in the ESI.†

3.4.1 3,3,6,6-Tetramethyl-9-phenyl-3,4,6,7,9,10-hexahydroacridine-1,8(2*H*,5*H*)-dione (4a). IR (ATR, ν cm^{-1}): 661, 833, 1035, 1154, 1237, 1363, 1582, 1630, 2956, 3286. ^{1}H NMR (400 MHz, $CDCl_3$) δ_H (ppm) = 1.09 (s, 6H, 2 × CH_3); 1.24 (s, 6H, 2 × CH_3), 2.51–2.33 (m, 8H, 4 × CH_2), 5.55 (s, 1H, CH), 7.11 (d, J = 8.2 Hz, 2H, Ar-H), 7.19 (d, J = 6.9 Hz, 2H, Ar-H), 7.26 (s, 1H, Ar-H), 7.27 (s, 1H, NH). ^{13}C NMR (100 MHz, $CDCl_3$) δ_C (ppm) = 27.5, 29.8, 31.5, 32.8, 47.1, 115.7, 125.9, 126.8, 128.1, 138.1, 189.5, 190.6.

4. Conclusion

In conclusion, we have successfully synthesized a novel Keggin-type molybdo-substituted tungstophosphoric acid ($H_3PW_7Mo_5O_{40} \cdot 12H_2O$) catalyst, which has been impregnated with acidified bentonite clay. The catalytic activity of PW_7Mo_5/bentonite was probed using the one-pot synthesis of the 1,8-dioxo-octahydroxanthene and 1,8-dioxo-decahydroacridine derivatives. The 20% PW_7Mo_5/bentonite exhibited a higher catalytic activity than the bulk PW_7Mo_5 catalyst, as well as 10%, 15% and 25% PW_7Mo_5/bentonite. The effects of various parameters, such as the catalyst loading, amount of catalyst, effect of the solvents, influence of the temperature on the rate of reaction, comparison of different catalysts and green metrics, were discussed in detail. The PW_7Mo_5/bentonite at 20% was found to be the most active, stable, and reusable catalyst. The PW_7Mo_5/bentonite catalysts have great potential for application as profitable catalysts for encouraging acid-catalysed organic transformations under environmentally friendly conditions and processes.

Conflicts of interest

There are no conflicts to declare.

Acknowledgements

The author SGS is thankful for financial assistance in the form of a minor research project (STAT/VI/RG/DEPT/2019–20/337–38) and UGC-DST SAP from Dr B. A. Marathwada University, Aurangabad (MS), India. The author DSA gratefully acknowledges the University Grants Commission (UGC), New Delhi (India) for a senior research fellowship (SRF).

References

1 X. Liu, Y. Zhang, G. Zhao, J. Zhang, S. Ren and G. Fang, *ACS Omega*, 2019, **4**, 18487–18494.

2 A. Enferadi-Kerenkan, T.-O. Do and S. Kaliaguine, *Catal. Sci. Technol.*, 2018, **8**, 2257–2284.
3 E. Rafiee and S. Eavani, *RSC Adv.*, 2016, **6**, 46433–46466.
4 J. Lan, J. Lin, Z. Chen and G. Yin, *ACS Catal.*, 2015, **5**, 2035–2041.
5 Y. Zhang, Z. Shen, J. Tang, Y. Zhang, L. Kong and Y. Zhang, *Org. Biomol. Chem.*, 2006, **4**, 1478–1482.
6 D. Borkin, E. Morzhina, S. Datta, A. Rudnitskaya, A. Sood, M. Torok and B. Torok, *Org. Biomol. Chem.*, 2011, **9**, 1394–1401.
7 H. Aghayan, A. R. Khanchi, T. Yousefi and H. Ghasemi, *J. Nucl. Mater.*, 2017, **496**, 207–214.
8 H. Wu, M. Zhou, Y. Qu, H. Li and H. Yin, *Chin. J. Chem. Eng.*, 2009, **17**, 200–206.
9 A. O. Terent'Ev, I. A. Yaremenko, V. A. Vil', I. K. Moiseev, S. A. Kon'Kov, V. M. Dembitsky, D. O. Levitsky and G. I. Nikishin, *Org. Biomol. Chem.*, 2013, **11**, 2613–2623.
10 C. Tagusagawa, A. Takagaki, K. Takanabe, K. Ebitani, S. Hayashi and K. Domen, *J. Phys. Chem. C*, 2009, **113**, 17421–17427.
11 J. Xu, R. W. Gable and C. Ritchie, *Acta Crystallogr., Sect. C: Struct. Chem.*, 2018, **74**, 1384–1389.
12 E. Rezaei-Seresht, F. M. Zonoz, M. Estiri and R. Tayebee, *Ind. Eng. Chem. Res.*, 2011, **50**, 1837–1846.
13 L. R. V. da Conceicao, L. M. Carneiro, D. S. Giordani and H. F. de Castro, *Renewable Energy*, 2017, **113**, 119–128.
14 L. D. Chavan and S. G. Shankarwar, *Chin. J. Catal.*, 2015, **36**, 1054–1059.
15 N. C. Coronel, M. J. da Silva, S. O. Ferreira, R. C. da Silva and R. Natalino, *ChemistrySelect*, 2019, **4**, 302–310.
16 J. E. Molinari, L. Nakka, T. Kim and I. E. Wachs, *ACS Catal.*, 2011, **1**, 1536–1548.
17 H. Cai, X. Wu, Q. Wu and W. Yan, *Dalton Trans.*, 2016, **45**, 14238–14242.
18 J. Li, X. Wang, W. Zhu and F. Cao, *ChemSusChem*, 2009, **2**, 177–183.
19 Z. Xie, H. Wu, Q. Wu and L. Ai, *RSC Adv.*, 2018, **8**, 13984–13988.
20 L. Rozic, B. Grbic, N. Radic, S. Petrovic, T. Novakovic, Z. Vukovic and Z. Nedic, *Appl. Clay Sci.*, 2011, **53**, 151–156.
21 V. V. Bokade and G. D. Yadav, *Appl. Clay Sci.*, 2011, **53**, 263–271.
22 G. Yadav, *J. Catal.*, 2003, **217**, 88–99.
23 L. Y. Zhang, S. Y. Cai, J. H. Mo, G. T. Wei, Z. M. Li, R. C. Ye and X. M. Xie, *Mater. Manuf. Processes*, 2015, **30**, 279–284.
24 A. d. N. de Oliveira, M. A. Barbosa de Lima, L. H. de Oliveira Pires, M. Rosas da Silva, P. T. Souza da Luz, R. S. Angelica, G. N. da Rocha Filho, C. E. F. da Costa, R. Luque and L. A. Santos do Nascimento, *Materials*, 2019, **12**, 1431.
25 D. S. Moraes, R. S. Angélica, C. E. F. Costa, G. N. Rocha Filho and J. R. Zamian, *Appl. Clay Sci.*, 2010, **48**, 475–480.
26 R. Liu, X. Xia, X. Niu, G. Zhang, Y. Lu, R. Jiang and S. He, *Appl. Clay Sci.*, 2015, **105–106**, 71–77.
27 R. A. Valiulin, L. M. Halliburton and A. G. Kutateladze, *Org. Lett.*, 2007, **9**, 4061–4063.
28 A. Domling, W. Wang and K. Wang, *Chem. Rev.*, 2012, **112**, 3083–3135.
29 Y. Liu, X. H. Zhang, J. Ren and G. Y. Jin, *Synth. Commun.*, 2004, **34**, 151–157.
30 S. Brauch, S. S. van Berkel and B. Westermann, *Chem. Soc. Rev.*, 2013, **42**, 4948.
31 Subodh, N. K. Mogha, K. Chaudhary, G. Kumar and D. T. Masram, *ACS Omega*, 2018, **3**, 16377–16385.
32 G. Shabir, A. Saeed and P. Ali Channar, *Mini-Rev. Org. Chem.*, 2018, **15**, 166–197.
33 S. A. Hilderbrand and R. Weissleder, *Tetrahedron Lett.*, 2007, **48**, 4383–4385.
34 B. B. Bhowmik and P. Ganguly, *Spectrochim. Acta, Part A*, 2005, **61**, 1997–2003.
35 R. Singh and G. Panda, *Org. Biomol. Chem.*, 2010, **8**, 1097.
36 S. Girault, P. Grellier, A. Berecibar, L. Maes, E. Mouray, P. Lemière, M.-A. Debreu, E. Davioud-Charvet and C. Sergheraert, *J. Med. Chem.*, 2000, **43**, 2646–2654.
37 C. Teixeira, N. Vale, B. Perez, A. Gomes, J. R. B. Gomes and P. Gomes, *Chem. Rev.*, 2014, **114**, 11164–11220.
38 A. Kumar, L. Rout, L. S. K. Achary, R. S. Dhaka and P. Dash, *Sci. Rep.*, 2017, **7**, 42975.
39 S. Hatakeyama, N. Ochi, H. Numata and S. Takano, *J. Chem. Soc., Chem. Commun.*, 1988, **64**, 1202–1204.
40 A. Amoozadeh, S. Rahmani, M. Bitaraf, F. B. Abadi and E. Tabrizian, *New J. Chem.*, 2016, **40**, 770–780.
41 M. Gensicka-Kowalewska, G. Cholewiński and K. Dzierzbicka, *RSC Adv.*, 2017, **7**, 15776–15804.
42 G. Rathee, S. Kohli, N. Singh, A. Awasthi and R. Chandra, *ACS Omega*, 2020, **5**, 15673–15680.
43 G. Song, B. Wang, H. Luo and L. Yang, *Catal. Commun.*, 2007, **8**, 673–676.
44 A. Ilangovan, S. Malayappasamy, S. Muralidharan and S. Maruthamuthu, *Chem. Cent. J.*, 2011, **5**, 81.
45 L. Q. Wu, Y. F. Wu, C. G. Yang, L. M. Yang and L. J. Yang, *J. Braz. Chem. Soc.*, 2010, **21**, 941–945.
46 X. Fan, X. Hu, X. Zhang and J. Wang, *Can. J. Chem.*, 2005, **83**, 16–20.
47 S. M. Vahdat, S. Khaksar, M. Akbari and S. Baghery, *Arabian J. Chem.*, 2019, **12**, 1515–1521.
48 M. Hong and G. Xiao, *J. Fluorine Chem.*, 2012, **144**, 7–9.
49 B. Das, P. Thirupathi, I. Mahender, V. S. Reddy and Y. K. Rao, *J. Mol. Catal. A: Chem.*, 2006, **247**, 233–239.
50 S. S. Kahandal, A. S. Burange, S. R. Kale, P. Prinsen, R. Luque and R. V. Jayaram, *Catal. Commun.*, 2017, **97**, 138–145.
51 K. Venkatesan, S. S. Pujari, R. J. Lahoti and K. V. Srinivasan, *Ultrason. Sonochem.*, 2008, **15**, 548–553.
52 A. N. Dadhania, V. K. Patel and D. K. Raval, *J. Saudi Chem. Soc.*, 2017, **21**, S163–S169.
53 K. Niknam, F. Panahi, D. Saberi and M. Mohagheghnejad, *J. Heterocycl. Chem.*, 2010, **47**, 292.
54 M. Dabiri, M. Baghbanzadeh and E. Arzroomchilar, *Catal. Commun.*, 2008, **9**, 939–942.
55 A. Ilangovan, S. Muralidharan, P. Sakthivel, S. Malayappasamy, S. Karuppusamy and M. P. Kaushik, *Tetrahedron Lett.*, 2013, **54**, 491–494.
56 F. Rashedian, D. Saberi and K. Niknam, *J. Chin. Chem. Soc.*, 2010, **57**, 998–1006.

57 P. S. Bhale, S. B. Dongare and Y. B. Mule, *Chem. Sci. Trans.*, 2015, **4**, 246–250.
58 Z. H. Zhang and Y. H. Liu, *Catal. Commun.*, 2008, **9**, 1715–1719.
59 Z.-H. Zhang and X.-Y. Tao, *Aust. J. Chem.*, 2008, **61**, 77.
60 D. S. Aher, K. R. Khillare, L. D. Chavan and S. G. Shankarwar, *ChemistrySelect*, 2020, **5**, 7320–7331.
61 D. S. Aher, K. R. Khillare, L. D. Chavan and S. G. Shankarwar, *RSC Adv.*, 2021, **11**, 2783–2792.
62 S. K. Bhorodwaj and D. K. Dutta, *Appl. Clay Sci.*, 2011, **53**, 347–352.
63 L. V. Chopda and P. N. Dave, *ChemistrySelect*, 2020, **5**, 2395–2400.
64 G. M. Ziarani, A. Badiei, M. Hassanzadeh and S. Mousavi, *Arabian J. Chem.*, 2014, **7**, 335–339.
65 M. Nasr-Esfahani, M. Montazerozohori and T. Abdizadeh, *C. R. Chim.*, 2015, **18**, 547–553.
66 T.-S. Jin, J.-S. Zhang, T.-T. Guo, A.-Q. Wang and T.-S. Li, *Synthesis*, 2004, **2004**, 2001–2005.
67 C. R. McElroy, A. Constantinou, L. C. Jones, L. Summerton and J. H. Clark, *Green Chem.*, 2015, **17**, 3111–3121.
68 R. A. Sheldon, *ACS Sustainable Chem. Eng.*, 2018, **6**, 32–48.
69 M. Tobiszewski, M. Marć, A. Gałuszka and J. Namieśnik, *Molecules*, 2015, **20**, 10928–10946.
70 R. A. Sheldon, *Green Chem.*, 2007, **9**, 1273.